International Journal of Pharmaceutics 403 (2011) 162–169

Contents lists available at ScienceDirect

International Journal of Pharmaceutics

journal homepage: www.elsevier.com/locate/ijpharm

Pharmaceutical Nanotechnology

# Development of biodegradable porous starch foam for improving oral delivery of poorly water soluble drugs

Chao Wu[a], Zhongyan Wang[b], Zhuangzhi Zhi[c], Tongying Jiang[a], Jinghai Zhang[d], Siling Wang[a,*]

[a] Department of Pharmaceutics, Shenyang Pharmaceutical University P.O. Box 32, 103 Wenhua Road, Shenhe District, Shenyang, Liaoning Province 110016, PR China
[b] Department of Physical Chemistry, School of Basic Science, Shenyang Pharmaceutical University, Wenhua Road 103, Shenyang, Liaoning Province 110016, PR China
[c] Department of Physics, School of Basic Science, Shenyang Pharmaceutical University, Wenhua Road 103, Shenyang, Liaoning 110016, PR China
[d] Key laboratory of Pharmaceutical Biotechnology, School of Life Science and Bio-Pharmaceutics, Shenyang Pharmaceutical University, Shenyang, Liaoning Province 110016, PR China

ARTICLE INFO

*Article history:*
Received 23 June 2010
Received in revised form 31 July 2010
Accepted 29 September 2010
Available online 16 October 2010

*Keywords:*
Biodegradable porous starch foam (BPSF)
Lovastatin
Bioavailability
Poorly water soluble drugs

ABSTRACT

A biodegradable porous starch foam (BPSF) was developed for the first time as a carrier in order to improve the dissolution and enhance the oral bioavailability of lovastatin – defined as a model poorly water soluble BCS type II drug. In this paper, BPSF was prepared by the solvent exchange method and characterized by scanning electron microscopy (SEM) and nitrogen adsorption/desorption analysis in order to perform the morphological and structural characterization of BPSF. Lovastatin was loaded by immersion/solvent evaporation into the BPSF which provided a stable hydrophilic matrix with a nano-porous structure. The solid state properties of the loaded BPSF samples were characterized by SEM, Fourier transform infrared spectroscopy (FTIR), X-ray powder diffraction (XRPD) and differential scanning calorimetry (DSC). In vitro and in vivo drug release studies showed that when BPSF was used as a carrier it allowed immediate release of lovastatin and enhanced the dissolution rate in comparison with crystalline lovastatin and commercial capsules. These results provide important information about the mechanism of drug adsorption and release from BPSF as a carrier. Accordingly, BPSF has a promising future as a device for the oral delivery of poorly water soluble drugs.



## 1. Introduction

Presently, there is considerable interest in improving the oral delivery of poorly water soluble drugs. In the Bio-pharmaceutic Classification System (BCS), low solubility and high permeability are the characteristics of BCS Class II poorly water soluble drugs. The low solubility markedly affects the oral bioavailability of such drugs, resulting in a nonideal therapeutic effect. Therefore, for BCS class II drugs, improving the solubility is the key to increasing the bioavailability. General methods to improving aqueous solubility of poorly water soluble drugs include the formation of inclusion complexes (Badr-Eldin et al., 2008), solid dispersions (Karavas et al., 2007; Tran et al., 2008), nanoparticles (Matteucci et al., 2007; Oh et al., 2010) or by controlling their polymorphic form (Masuda et al., 2006). At present, several inorganic materials, such as mesoporous silica (Zhang et al., 2010a,b; Huang et al., 2010; Shi et al., 2009; Kilpeläinen et al., 2009; Nunes et al., 2007), clay particles (Zhang et al., 2010a,b) and lipid–inorganic hybrids (Tan et al., 2009), have also been employed. These highly porous materials typically possess nano metre-sized pores and provide a large effective specific surface area and a hydrophilic surface. Due to spatial confinement within the nano metre-sized pores, crystalline drug molecules are normally unable to form highly ordered crystals, instead remaining in microcrystalline or amorphous forms.

In this context, BPSF, as a biodegradable starch-based porous biomaterial, has great potential as a solid dispersion carrier for oral poorly water soluble drugs, which is to date unexplored. BPSF presents excellent characteristics compared with inorganic carriers, and has a nano-porous structure, low density, high specific surface area and pore volume; its distinctive advantages are as follows: (1) nontoxicity, biocompatibility, biodegradability (Marques et al., 2002; Araujo et al., 2004); (2) new functional groups can be readily introduced to the main backbone of the starch foam because of the high number of hydroxyl groups on the surface of the starch; (3) soluble amylum as the raw material of BPSF is partially soluble in water, which facilitates the release of drug dispersed in the BPSF channels. These are particularly desirable properties for the design of carriers for the oral delivery systems of poorly water soluble drugs. Starch-based polymers have been extensively studied for many applications as drug carriers ranging from tissue engineering scaffolds (Duartea et al., 2009), to bone cements (Boesel

* Corresponding author. Tel.: +86 24 23986348; fax: +86 24 23986348.
*E-mail addresses:* silingwang@syphu.edu.cn, silingwang@hotmail.com (S. Wang).

0378-5173/$ – see front matter © 2010 Elsevier B.V. All rights reserved.
doi:10.1016/j.ijpharm.2010.09.040

et al., 2004), microparticle drug delivery systems (Jain et al., 2008; Santander-Ortega et al., 2010) and hydrogels (El-Hag Ali and AlArifi, 2009; Elviraa et al., 2002). It is clear that starch is the most reliable carrier material.

General starch foam is prepared by swelling using the extrusion (Lee et al., 2009) or microwave technique (Malafaya et al., 2001). The product of swelling using the extrusion or microwave technique has a large pore size $\geq$1 μm. In this paper, BPSF was formulated by gelatinization associated with the solvent exchange technique. Using this method, the obtained products have several advantages such as a smaller pore size of $\leq$200 nm, a generally high yield, high batch to batch reproducibility and easy scaling up.

In the last decade, scientists have successfully prepared numerous foam products including starch microcellular foams (SMCF) for encapsulation of volatile compounds (Glenn, 2008; Glenn et al., 2008), porous injection molded starch-based blends for tissue engineering scaffolding (Neves et al., 2005). However, there is not detailed study of the application of BPSF as a excipient to improve the aqueous solubility of poorly water soluble drugs.

This work was carried out to explore the use of BPSF as an administration system for poorly water soluble drugs, by using the advantages of the nanometre-porous structure, low density, high specific surface area and pore volume of BPSF in order to increase solubility of poorly water soluble drugs and improve their bioavailability. To achieve this, we selected lovastatin as a model poorly water soluble BCS type II drug and impregnation, adsorption and volatilization from a Lovastatin/BPSF chloroform solution was used for loading lovastatin into BPSF. The capacity of BPSF as a drug delivery system was demonstrated in vitro and in vivo tests. The solid state properties of the loaded BPSF samples were characterized by SEM, FTIR, XRPD and DSC in order to analyze dispersal state of the loaded lovastatin compare with pure lovastatin and commercial capsules. Hence, it is reasonable to examine the use of BPSF as an oral delivery system for poorly water soluble drugs.

## 2. Materials and methods

### 2.1. Chemicals and materials

Soluble starch and anhydrous ethanol were purchased from Shan Dong Yu Wang reagent company. Lovastatin was supplied by Wu Han Yuan Cheng company with a purity >99% and was used as received. Deionized water was used in all experiments. Commercial capsules were produced by Jiang Su Fei Ma company.

### 2.2. Preparation of BPSF

A selected amount of 8.0 wt.% soluble amylum and water suspension was heated to 100 °C for 0.5 h under stirring in a reaction vessel. The melt was lowered to 85 °C and then poured into a Petri dish. The resulting slurry was chilled in a refrigerator (5 °C) overnight to facilitate gelation. The gel was then transferred to five volumes of 40%, 60%, 90% and 100% ethanol/water solution, respectively and equilibrated for 24 h in order to maintain the porous structure of the gel, whereby ethanol displaced the water in the aquagel to form an alcogel. The resulting foam was obtained by rotary evaporation drying in 30 °C. The dry BPSF was milled in a mortar and passed through an 80 mesh sieve, and the BPSF particles were stored in a vaccum dryer.

### 2.3. Drug loading by immersion/solvent evaporation

Prior to the integration of lovastatin, BPSF was dried by rotary evaporation heating at 30 °C under vacuum for 0.5 h. According to the oral dose and specification of the commercial capsule (20 mg), lovastatin/chloroform solution (20 mg/ml) and BPSF in ratios of 1/5, 1/10, 1/15 were mixed and stirred for 5 h at room temperature. After vacuum drying, the solid powder was dried in a vaccum dryer for 24 h. Since the adsorption increased with an increase in concentration (Takeuchi et al., 2005), and lovastatin has maximum solubility in chloroform, so, chloroform was selected as the dissolution medium.

### 2.4. Preparation of physical mixture

The 1:5 ratio physical mixture of Lovastatin/BPSF was obtained by mixing the single components in a mortar until the mixture was homogeneous.

### 2.5. SEM characterization of BPSF and the loaded BPSF samples

The morphology and structure of BPSF and the loaded BPSF samples were examined using a field emission scanning electron microscope (JEOL JSM-7001F) operated at an accelerating voltage of 1 kV and a secondary detector.

### 2.6. Nitrogen adsorption/desorption analysis of BPSF

Nitrogen adsorption isotherms were obtained using a SA3100 surface area analyzer (Beckman coulter, USA). Powder samples ($\leq$200 mg) were transferred to the sample bulb and evacuated to a pressure of $10^{-4}$ Pa at 50 °C overnight (>12 h) to remove physically adsorbed water prior to analysis. The Brumauer–Emmet–Teller specific surface area (BET-SSA) was estimated from the nitrogen adsorption data over a relative pressure ($P/P_0$) range from 0.0 to 1.0. The pore size distributions and pore volumes were calculated by the Barrett–Joiner–Halenda (BJH) method.

### 2.7. DSC characterization of BPSF and the loaded BPSF samples

Samples were accurately weighed and encapsulated in flat-bottomed aluminium pans with crimped-on lids. The DSC patterns were obtained with a DSC-60 differential scanning calorimeter (Shimadzu, Japan). The measurements from 30 to 300 °C were obtained at a scanning speed of 10 °C/min under a nitrogen stream at a flow rate of 40 ml/min.

### 2.8. XRPD characterization of BPSF and the loaded BPSF samples

XRPD was carried out using a diffractometer (Rigaku Geigerflex XRD, Co., Japan) with Cu–Ka radiation ($\lambda$ = 1.54 Å) at 30 kV and 30 mA Philips. The monochromic diffraction beam was obtained with a LiF crystal. Powder samples were scanned over the angular range of 5° (2$\theta$) to 60° with a scan rate of 0.5°/min and a step size of 0.02°.

### 2.9. FTIR characterization of BPSF and the loaded BPSF samples

Fourier transform IR spectra were obtained using an FT-IR spectrometer (Bruker IFS 55, Switzerland) using the KBr pellet technique. The spectroscopic range from 400 to 4000 $cm^{-1}$ was investigated. In order to obtain a good signal-to-noise ratio (S/N) and high reproducibility, each spectrum was collected at a resolution of 2 $cm^{-1}$, and an average of 100 repetitive scans was automatically obtained for each run. All the measurements were performed in a dry atmosphere.

### 2.10. In vitro drug release studies of the loaded BPSF samples

Drug release was determined by evaluation of the cumulative dissolution percentage of drug released from BPSF, pure drug and commercial capsules using the USP dissolution apparatus

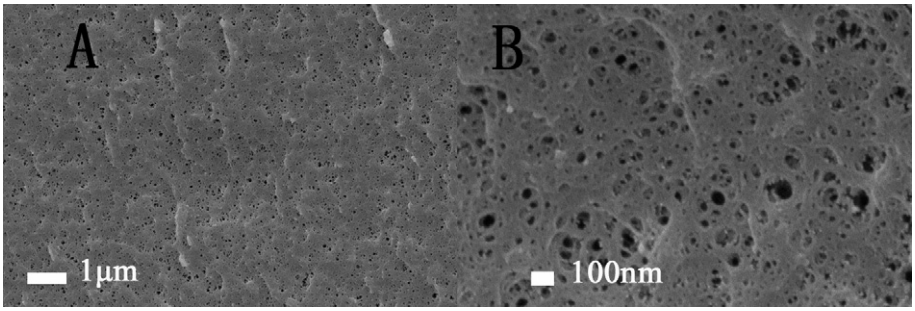


**Fig. 1.** The surface feature of cross-section of the BPSF (A and B).

type II (paddle) method (RC-8D, Tianjin Guoming Medical Equipment Co., Ltd.) in 900 ml phosphate buffer pH 7.0 with 0.2% SDS at a dissolution medium temperature of 37 ± 0.5 °C (Mehramizi et al., 2007). The amount of the drug was chosen so that the final concentration was equal to 10% of the maximal solubility of this drug in 0.2% SDS (sink conditions). The medium was agitated at 50 rpm and samples were taken at specified times (5, 10, 15, 20, 30, 45 min) and the lovastatin content was determined at 238 nm by ultraviolet spectrophotometry (UV-2000, Unico, USA). The mean of three determinations was used to calculate the amount of drug released from the sample. The amount of drug released was plotted versus time as a percentage of dissolved drug.

### 2.11. In vivo pharmacokinetics

The in vivo experiments were performed on male Sprague–Dawley rats (250 ± 20 g). The animal experiment protocol was reviewed and approved by the Institutional Animal Care and Use Committee of Shen Yang Pharmaceutical University. Animals were housed and handled according to institutional guidelines. All animals were fasted overnight prior to the experiments. All rats were lightly anesthetized with diethyl ether. Lovastatin was given orally (100 mg/kg) (Chen et al., 2010) and oral formulations were delivered by gavage. Blood samples (each 500 μl) were obtained by retroorbital venous plexus puncture at 15, 30, 45, 60, 90,120, 240 and 360 min after dosing (Suresh et al., 2007). The samples were collected in heparinized Eppendorf tubes and centrifuged at 8000 g for 10 min and the collected plasma was stored at −20 °C until analysis. For analysis, plasma samples (200 μl) were vortex-mixed with 20 μl internal standard (simvastatin, 5 μg/ml) in methanol and acetic ether/acetone solution (1:4, 800 μl). The denatured protein precipitate was separated by centrifugation at 10000 rpm for 10 min. Then, each supernatant was transferred to an Eppendorf tube (1.5 ml) and dried under vacuum using a centrifugal drying machine (Labconco Corporation, Kansis City, MO). Residues were reconstituted in 50 μl of the combined eluate of methanol–water (80:20), and then vortexed for 5 min. The reconstituted samples (20 μl) were injected into an HPLC for analysis [mobile phase methanol–water (80:20), flow rate (1 ml/min)]. Over the range 0.031–6.12 μg/ml, the concentration of lovastatin was linearly proportional to the chromatographic peak area/internal standard area (correlation >0.994).

### 2.12. Statistical analysis

All data were expressed as averages with standard deviations. In vivo test pair-wise comparison was made using Excel's *t*-test. A *p*-value of <0.05 was considered statistically significant.

## 3. Results and discussion

### 3.1. Preparation of BPSF

In this study, we used the solvent exchange method to prepare BPSF. The exchange solvent is an important factor to displace water from the hydrogel to maintain the porous structure of the gel. So, we selected alcohol as the exchange solvent to avoid contraction and collapse of the aquagel due to direct air drying. According to surface tension formulation ($\gamma = a - bt$, $a$, $b$ represent constant, $t$ represents temperature), the $a$ and $b$ of alcohol is 24.05 and 0.1549 compared with 78.97 and 0.0832 of water. It is obvious that alcohol has a lower surface tension than water, and does not solubilize starch and can be readily volatilized compared with other nonaqueous solvents. The type of starch and heating temperature and the concentration of the aqueous starch solution also have a close relationship with the properties of BPSF. The porous structure absorbs lovastatin by immersion/solvent evaporation. Mechanisms of the drug adsorption due to solvent evaporation involves a number of pore scale mechanisms, including mass transfer by advection and diffusion in the gas phase, viscous flow in the liquid and gas phases and capillary effects at the gas–liquid menisci in the pore throats (Yiotis et al., 2001).

### 3.2. The morphological and structural characterization of BPSF

The morphological and structural features of BPSF are further examined by SEM. As shown in Fig. 1 SEM images clearly show that BPSF with a nanometre porous structure (≤200 nm) is obtained from all the samples. The cross-connection between pores is a clear advantage. Firstly, it can increase the specific surface area,

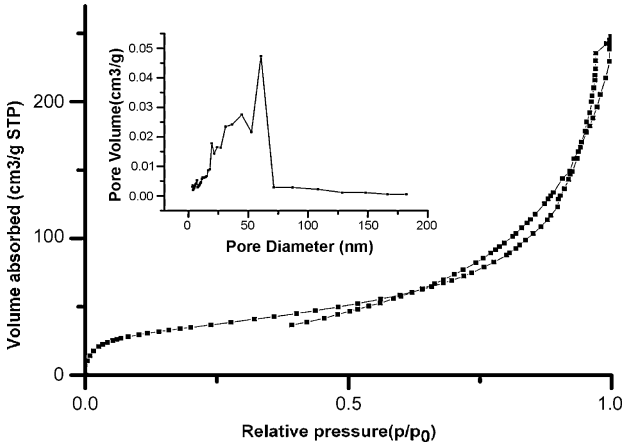


**Fig. 2.** The N2 adsorption–desorption isotherms and pore size distribution curve (BJH) of BPSF.

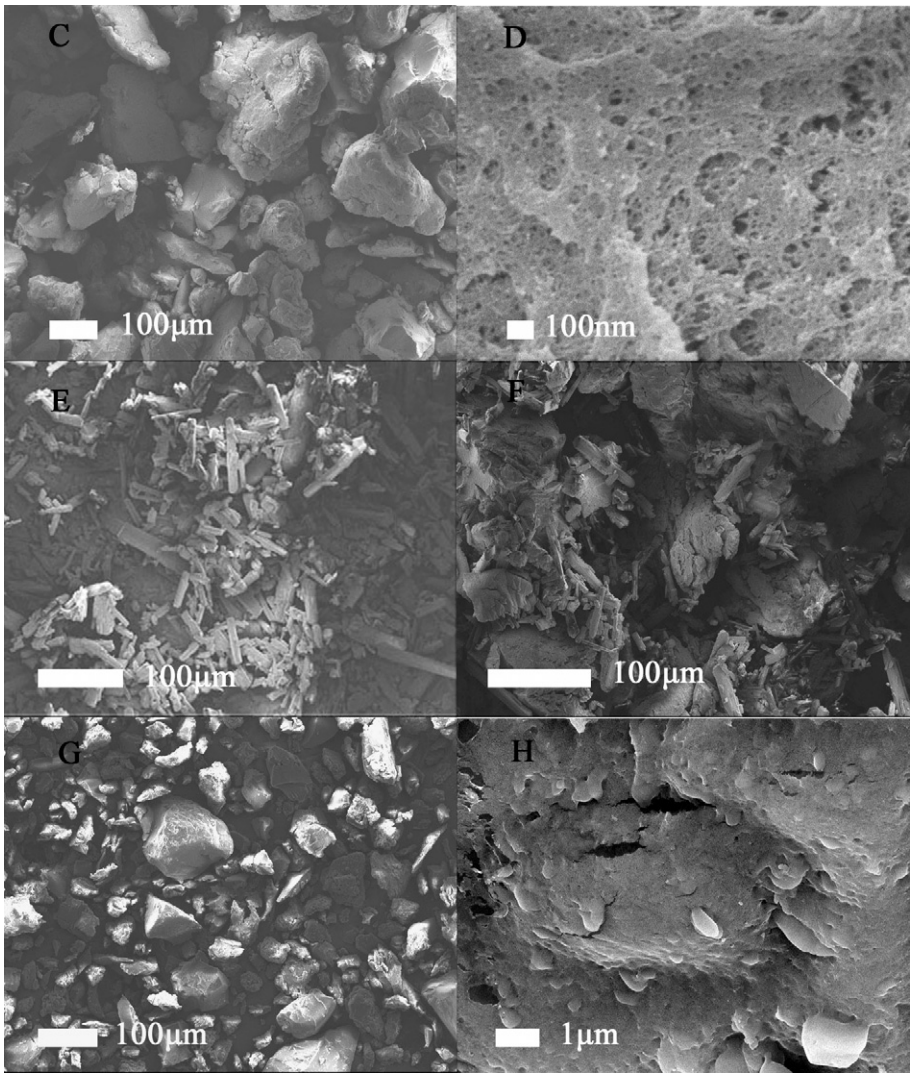


**Fig. 3.** The SEM images of BPSF particle after milling(C) and (D), crude drug (E), physical mixture (F), and the loaded BPSF particles (G) and (H).

maintain the size of the drug particles in the nanometre range, prevent congestion and agglomerate the drug particles, while maintaining the dispersion of the particles, reducing the crystallinity of the drug and enhancing its physical stability. Secondly, drug is absorbed into the pores from different directions and this simultaneously reduces the diffusional resistance of drug in the porous channels. All these features promote drug dissolution.

### *3.3. Estimation of specific surface area and pore size distribution from N2 adsorption/desorption studies*

As seen in Fig. 2, the N2 adsorption–desorption isotherms of BPSF suggest that the pore shape resembles a type IV isotherm with an N2 hysteresis loop at different opening and closing pressures (Rouquerol et al., 1994). Two hysteresis loops appear in the relative pressure ranges from 0.6–0.8 to 0.8–1.0 ($P/P_0$), which are related to the filling and emptying of mesopores by capillary condensation. The first loop at 0.6–0.8 is due to capillary condensation within mesopores. The second loop may arise from macropore. The BJH pore size distribution of BPSF is shown in Fig. 2. The pore size distribution of BPSF is narrow (≤200 nm) and 60% of the BPSF pores have a diameter of 20–80 nm. The pore size distribution of BPSF is between that of meso pores and large pores, in consistent with the SEM images (Fig. 1A and B). The BET specific surface area and total pore volume are calculated to be 127.75 $m^2/g$ and 0.38 ml/g.

### *3.4. Physicochemical characterization of the loaded BPSF samples*

The loading of the drug on the carrier depends not only on the properties of the drug itself but also on the physical properties of the carrier. Lovastatin incorporated in BPSF via immersion/solvent evaporation is characterized by SEM, XRPD, DSC and IR.

#### *3.4.1. SEM characterization*

Porous structure of BPSF particle after milling is not destroyed in Fig. 3C and D. As is shown in Fig. 3E, the crystalline crude drug (lovastatin) is in the form of regular rod-shaped particles. A physical mixture of crude drug and BPSF is dispersed as shown in Fig. 3F. However, the loaded sample does not exist rod-shaped crystal and pores are completely filled with drug as shown in Fig. 3G and H. This indicates that some lovastatin is present on surface of BPSF, some in the BPSF pores.

#### *3.4.2. XRPD characterization*

The XRPD patterns of BPSF and the loaded BPSF samples are shown in Fig. 4. For comparison, we added the pattern of pure lovas-

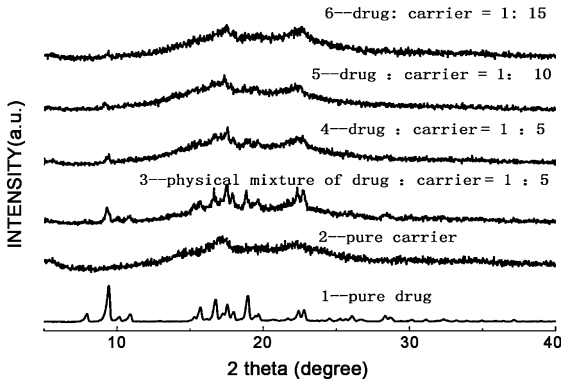


**Fig. 4.** The XRPD powder patterns of BPSF, pure lovastatin, its physical mixtures and the loaded BPSF samples.

tatin and the physical mixture of lovastatin and BPSF. For pure BPSF, the characteristic peaks are in the same position as raw starch. The crystallinity of BPSF and raw starch are calculated using origin 8.0 software as 26.76% and 28.6%, respectively. This indicates that the hardness of BPSF does not change in comparison with raw starch. From the XRPD patterns of the loaded samples in Fig. 4, the loaded sample (1/5 Lovastatin/BPSF) has a markedly lower intensity than the physical mixture with the same ratio, which illustrates that crystallization of lovastatin is reduced by adsorption of BPSF. The XRPD patterns of lovastatin in loaded samples are reduced on increasing the amount of BPSF. Moreover, according to the Scherrer formula (Kapoor et al., 2009), the change in grain size is evident from the representative peak at $2\theta = 9.4°$. It was 19.739 nm 14.993 nm, 11.314 nm, 29.644 nm, and 38.325 nm corresponding to 1:5 Lovastatin/BPSF, 1:10 Lovastatin/BPSF, 1:15 Lovastatin/BPSF, 1:5 physical mixture of Lovastatin/BPSF, crude lovastatin. The grain size of lovastatin loaded in BPSF is smaller compared with crude lovastatin. These results confirm that the specific surface area of the particles is significantly increased, which is a main reason for improving the dissolution. It is also found that lovastatin absorbed in pores or edges is partially present as microcrystals, partially amorphously distributed on account of wide pore size distribution of BPSF range from micropores, to mesopores and large pores. On the surface of BPSF, lovastatin is still present in crystal form.

### 3.4.3. *Differential scanning calorimetry (DSC) characterization*

As seen in Fig. 5, the melting point of crude lovastatin is 175.35 °C. Its corresponding physical mixture with BPSF and pure

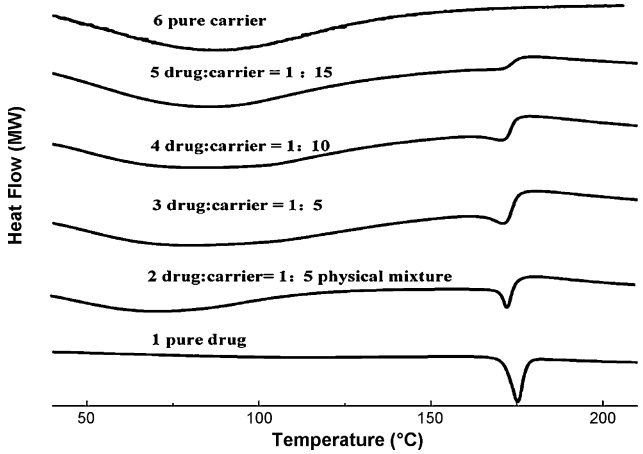


**Fig. 5.** DSC patterns of BPSF, pure lovastatin, its physical mixtures and the loaded BPSF samples.

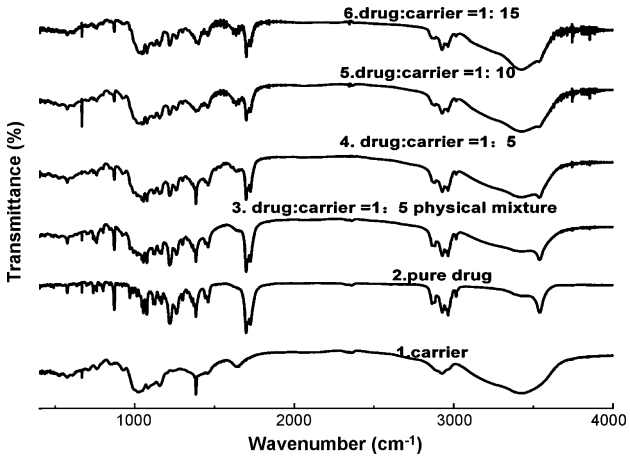


**Fig. 6.** The FTIR spectra obtained for BPSF, pure lovastatin, physical mixture and the loaded BPSF samples.

BPSF are shown in comparison with the loaded samples. The loaded sample (1/5 Lovastatin/BPSF) has a wider and weaker melting peak than the physical mixture with the same ratio and the melting peak of lovastatin with an increased proportion of BPSF is also wider and weaker. The onset temperature of physical mixture (1/5 Lovastatin/BPSF) and pure drug is 170.26 °C and 170.80 °C while that of the corresponding loaded samples with an increased proportion of BPSF is 166.27 °C,165.07 °C and 162.25 °C corresponding to 1:5 Lovastatin/BPSF, 1:10 Lovastatin/BPSF, 1:15 Lovastatin/BPSF, respectively. The peak temperature (170.45 °C) of the loaded samples is approximately 5 °C lower than the pure drug (175.35 °C). This indicates a change in the crystallinity of lovastatin absorbed in BPSF. The results of DSC in Fig. 5 also support the results obtained by XRPD.

### 3.4.4. *Fourier-transform infrared spectroscopy characterization*

The FTIR spectra obtained for BPSF, crude lovastatin, the physical mixture and the loaded samples are presented in Fig. 6. Typical features of the loaded samples compared with the physical mixture of BPSF and crude lovastatin show no new peaks or migration of the characteristic peak position, demonstrating that there is no interaction between lovastatin and BPSF. These results indicate that the absorption of lovastatin in BPSF is physical. Moreover, the BPSF FTIR spectra have the peaks at 3000–3500 $cm^{-1}$ (–OH stretching), which show that BPSF also has a hydrophilic surface with lots of hydrophilic hydroxyl groups. The carbonyl peak of lovastatin at 1725.8 $cm^{-1}$ in the loaded sample (1/5 Lovastatin/BPSF) is weaker than that of the physical mixture with the same ratio and the melting peak of lovastatin is also lower on increasing the proportion of BPSF. The fine particles of BPSF are very efficient at scattering light and have a strong opacifying ability because BPSF has a very high specific area (air–solid interfaces) for scattering light (El-Tahlawy et al., 2007). Therefore, lovastatin on the BPSF surface is only detected by FTIR. The loaded sample (1/5 Lovastatin/BPSF) has a clearly lower carbonyl peak intensity than the physical mixture with the same ratio, which shows that lovastatin is loaded into the BPSF pores. However, some lovastatin remains coat on the BPSF surface.

## 3.5. *In vitro drug release studies of the loaded BPSF samples*

It is found that the use of hydrophilic BPSF as a carrier for poorly water soluble drugs produced a fast release of lovastatin. As shown in Fig. 7, lovastatin loaded into BPSF exhibit a rapid release of 80% within 15 min in comparision to 45 min for the current commercial product with the same ratio. Lovastatin loaded into the inner chan-

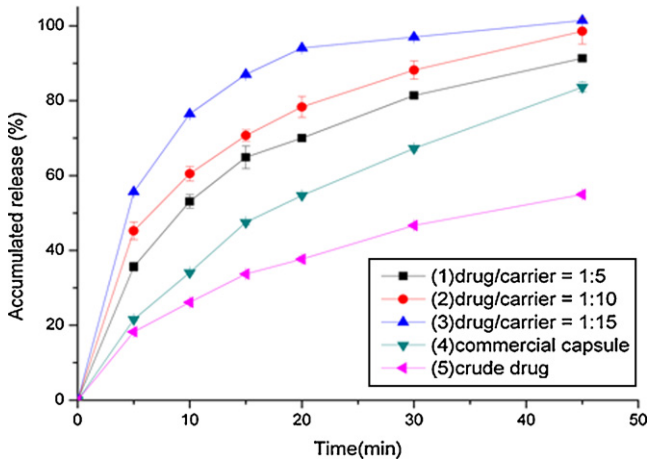


**Fig. 7.** In vitro drug cumulative dissolution percentage patterns of the loaded BPSF samples, crude drug and commercial capsule. The data represent the average results of three independent batches. Error bars are standard deviations and not seen in some data points as they are smaller than the symbols. $^{*}p < 0.05$ and $^{**}p < 0.01$ indicate statistical difference at each time point.

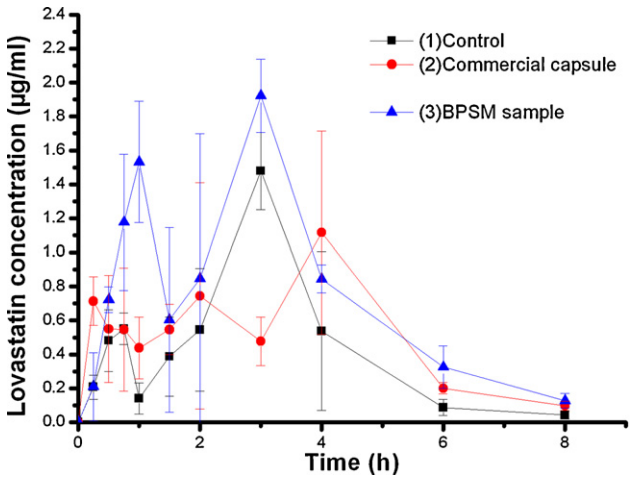


**Fig. 8.** The concentration versus time profiles of the free control, commercial capsule and the loaded sample (drug/carrier, 1/10).

nels and on the surfaces of BPSF exhibit a different release pattern: in the first 5 min approximately 50% of the lovastatin is released, showing a significant burst release effect, while the remainder follow a typical sustained release pattern and dissolve quickly and evenly over a period of 40 min. In Table 1, according to zero-order, first-order and Higuchi kinetic equation, the fitting of the release data indicates that rate constant of the loaded BPSF samples is significantly higher than that of the commercial capsules and pure drug and agrees well with first-order kinetics. Pure drug has lowest release rate and rate constant. This effect can be explained by both an increase in the specific surface area of microcrystalline lovastatin adsorbed in the BPSF and its non-crystalline structure in this state. Another important aspect is the partial solution and collapse of BPSF structure in water. Hydrophilic BPSF is rapidly wetted with water so that the drug molecules are surrounded with water, allowing fast drug dissolution. Enzymes in the alimentary tract attack BPSF, which also leads to collapse of BPSF structure and release of drug.

The drug release process from hydrophilic BPSF is dominated mainly extent by the sudden influx of water, which leads to a fast release. Thus, both the loading of BPSF with drug and its release rate can be influenced by the properties of BPSF. Hydrophilic BPSF used as a carrier material accelerates the dissolution of poorly water soluble drugs, such as lovastatin, and thus improves their bioavailability.

### 3.6. *In vivo* pharmacokinetics

Fig. 8 illustrates the concentration versus time profiles of lovastatin following the administration of a single oral dose to three groups, including the free control (pure lovastatin), commercial capsule and the loaded sample (drug/carrier, 1/10). The pharmacokinetic parameters obtained by a non-compartmental analysis after the oral administration of lovastatin are listed in Table 2. The AUC (0–$t$) value of lovastatin after oral gavage of the loaded sample drug/carrier (1/10) is respectively 1.773- and 1.480-fold higher than that obtained with the free control and commercial capsule. As shown in Fig. 8, in comparison with the free control and commercial capsule exhibiting a weak double peak concentration distribution, the loaded sample has an intensive double peak concentration and the first peak concentration is higher than the second. This may be due to two factors. (i) Lovastatin is loaded into the inner channel and on the surface of BPSF. Lovastatin adsorbed on the surface of BPSF is still present as crystals while lovastatin adsorbed in the inner channels of BPSF is partially present as microcrystals and partially in a non-crystalline state due to geometric confinement in the nanometre sized pores. The crystalline state of lovastatin may produce two absorption patterns which may be the reason for the appearance of a double peak. Firstly, microcrystals and non-crystalline lovastatin accelerate the dissolution of lovastatin. The released lovastatin molecules are directly absorbed by enterocytes into the blood capillaries which result in the first peak concentration. Secondly, lymphatic transport may be the reason for the second peak concentration. Lovastatin (the water solubility of which is $0.4 \times 10^{-3}$ mg/ml) is considered to be a reasonable substrate for intestinal lymphatic transport because of its high lipophilicity. The gastrointestinal tract contains absorptive enterocytes interspersed with membranous epithelial (M) cells. M cells covering lymphoid aggregates, defined as Peyer's patches, take up lipophilic microcrystalline particles by a combination of endocytosis or transcytosis (Norris et al., 1998; Andrianov and Payne, 1998). Microcrystalline lovastatin in the pore interior or the edge of BPSF are released from pores and ingested by lymphatic transport. The absorption efficiency is directly related to the size of the crystalline particles of lovastatin. Mucoadhesion also play a role in absorption. BPSF absorbs water and expands to form colloidal

**Table 1**
Results for fitting lovastatin release data (in the range 0–100% release) to zero-order, first-order and Higuchi kinetic equations.

| | Zero order kinetic equation | | First order kinetic equation | | Higuchi equation | |
|---|---|---|---|---|---|---|
| | $K$ | $R^2$ | $K$ | $R^2$ | $K$ | $R^2$ |
| 1:5 drug/BPSF | 1.7707 | 0.7910 | 0.0519 | 0.9879 | 13.8880 | 0.9764 |
| 1:10 drug/BPSF | 1.8463 | 0.7551 | 0.0875 | 0.9675 | 14.7290 | 0.9644 |
| 1:15 drug/BPSF | 1.7784 | 0.5961 | 0.1008 | 0.9704 | 15.2020 | 0.8741 |
| Commercial capsule | 1.7514 | 0.9277 | 0.0390 | 0.9949 | 12.7820 | 0.9916 |
| Crude drug | 1.1121 | 0.8846 | 0.0167 | 0.9537 | 6.9643 | 0.9412 |

**Table 2**
Pharmacokinetic parameters of lovastatin (100 mg/kg) after oral administration of free control, commercial capsule and the loaded sample.

| Parameter | Control | Commercial capsule | Loaded BPSF preparation |
|---|---|---|---|
| Cmax (mg/L)[a] | 1.479 ± 0.227 | 1.441 ± 0.403 | 3.032 ± 0.691 |
| Tmax (h)[b] | 3.020 ± 0.502 | 2.625 ± 1.702 | 1.002 ± 0.496 |
| AUC(0–*t*) (mg/L h)[c] | 3.464 ± 1.082 | 4.148 ± 1.070 | 6.140 ± 1.628 |
| MRT (h)[d] | 2.946 ± 0.273 | 3.179 ± 0.210 | 2.352 ± 0.209 |
| *t*1/2 (h)[e] | 1.340 ± 0.389 | 1.871 ± 0.395 | 1.911 ± 0.726 |
| Vz/F (L/kg)[f] | 57.006 ± 21.384 | 63.238 ± 14.140 | 36.994 ± 10.247 |

Each value represents the mean ± SD ($n = 6$).
[a] Maximum plasma concentration.
[b] Time to reach Cmax.
[c] Area under the plasma concentration–time curve.
[d] Mean residence time.
[e] Elimination half-life.
[f] Apparent volume of distribution.

material which undergoes mucoadhesion. Following destruction by enzymes in the small intestine, degradation of BPSF facilitates the release of lovastatin which leads to further accelerated absorption. (ii) distribution; drug is absorbed into the blood and produces the first peak. Because the drug is highly lipophilic, after absorption, it rapidly distributes to lipid tissue which acts as a drug storage compartment. When the drug concentration in the blood is reduced following metabolism and elimination, the drug in this compartment is redistributed into blood again, resulting in the formation of a second peak. Hepatoenteral circulation may also be a factor involved in generating the double peak. The exact mechanism of the metabolism of BPSF loaded samples needs further study.

## 4. Conclusions

A biodegradable porous starch foam (BPSF) possesing a low density, high specific surface area, honeycomb structure, and high pore volume for the oral delivery of poorly soluble drugs was obtained and its structure was determined by SEM, BET. SEM, XRD, DSC and FTIR characterization showed that lovastatin absorbed on BPSF was partially present as microcrystals, and partially in amorphous form distributed in the pores of BPSF and partially in crystalline form distributed on the surface of BPSF. In vitro and in vivo drug release studies showed that the BPSF carrier produced accelerated immediate release of lovastatin and enhanced its oral bioavailability in comparison with crude lovastatin and commercial capsules. From these findings, this study demonstrates the significant potential for the use of BPSF as a novel delivery system for poorly water soluble drugs. This method can be applied as an alternative to other method currently used to enhance the solubility of poorly soluble drugs in the BCS (class 2), i.e. poor solubility/high permeability.

## Acknowledgment

This work was supported by the National Basic Research Program of China (973 Program) (No. 2009CB930300).

## References

Andrianov, A.K., Payne, L.G., 1998. Polymeric carriers for oral uptake of microparticulates. Adv. Drug. Deliv. Rev. 34, 155–170.
Araujo, M.A., Cunha, A.M., Mota, M., 2004. Enzymatic degradation of starch-based thermoplastic compounds used in protheses: identification of the degradation products in solution. Biomaterials 25, 2687–2693.
Badr-Eldin, S.M., Elkheshen, S.A., Ghorab, M.M., 2008. Inclusion complexes of tadalafil with natural and chemically modified b-cyclodextrins I: preparation and in vitro evaluation. Eur. J. Pharm. Biopharm. 70, 819–827.
Boesel, L.F., Mano, J.F., Reis, R.L., 2004. Optimization of the formulation and mechanical properties of starch based partially degradable bone cements. J. Mater. Sci. Mater. Med. 15, 73.
Chen, C.C., Tsai, T.H., Huang, Z.R., Fang, J.Y., 2010. Effects of lipophilic emulsifiers on the oral administration of lovastatin from nanostructured lipid carriers: physicochemical characterization and pharmacokinetics. Eur. J. Pharm. Biopharm. 74, 474–482.
Duartea, A.R.C., Mano, J.F., Reis, R.L., 2009. Preparation of starch-based scaffolds for tissue engineering by supercritical immersion precipitation. J. Supercrit. Fluids 49, 279–285.
El-Hag Ali, A., AlArifi, A., 2009. Characterization and in vitro evaluation of starch based hydrogels as carriers for colon specific drug delivery systems. Carbohydr. Polym. 78, 725–730.
El-Tahlawy, K., Venditti, R.A., Pawlak, J.J., 2007. Aspects of the preparation of starch microcellular foam particles crosslinked with glutaraldehyde using a solvent exchange technique. Carbohydr. Polym. 67, 319–331.
Elviraa, C., Manoa, J.F., San Roman, J., Reisa, R.L., 2002. Starch-based biodegradable hydrogels with potential biomedical applications as drug delivery systems. Biomaterials 23, 1955–1966.
Glenn, G.M., 2008. Starch foam microparticles. US Patent No. 0131538A1.
Glenn, G.M., Imam, S.H., Klamczynski, A.P., Chiou, B.S., Wood, D.F., Orts, W.J., 2008. Structure of porous starch microcellular foam particles. Microsc. Microanal. 14, 150–151.
Huang, X.L., Teng, X., Chen, D., Tang, F.Q., He, J.Q., 2010. The effect of the shape of mesoporous silica nanoparticles on cellular uptake and cell function. Biomaterials 31, 438–448.
Jain, A.K., Khar, R.K., Ahmed, F.J., Diwan, P.V., 2008. Effective insulin delivery using starch nanoparticles as a potential trans-nasal mucoadhesive carrier. Eur. J. Pharm. Biopharm. 69, 426–435.
Kapoor, S., Hegde, R., Bhattacharyya, A.J., 2009. Influence of surface chemistry of mesoporous alumina with wide pore distribution on controlled drug release. J. Control. Release 140, 34–39.
Karavas, E., Georgarakis, E., Sigalas, M.P., Avgoustakis, K., Bikiaris, D., 2007. Investigation of the release mechanism of a sparingly water-soluble drug from solid dispersions in hydrophilic carriers based on physical state of drug, particle size distribution and drug–polymer interactions. Eur. J. Pharm. Biopharm. 66, 334–347.
Kilpeläinen, M., Riikonen, J., Vlasova, M.A., Huotari, A., Lehto, V.P., Salonen, J., et al., 2009. In vivo delivery of a peptide, ghrelin antagonist, with mesoporous silicon microparticles. J. Control. Release 137, 166–170.
Lee, S.Y., Eskridge, K.M., Koh, W.Y., Hanna, M.A., 2009. Evaluation of ingredient effects on extruded starch-based foams using a supersaturated split–plot design. Ind. Crop. Prod. 29, 427–436.
Malafaya, P.B., Elvira, C., Gallardo, A., San Roman, J., Reis, R.L., 2001. Porous starch-based drug delivery systems processed by a microwave route. J. Biomater. Sci. Polym. Ed. 12, 1227–1241.
Marques, A.P., Reis, R.L., Hunt, J.A., 2002. The biocompatibility of novel starch-based polymers and composites: in vitro studies. Biomaterials 23, 1471–1478.
Masuda, K., Tabata, S., Kono, H., Sakata, Y., Hayase, T., Yonemochi, E., Terada, K., 2006. Solid-state $^{13}$C NMR study of indomethacin polymorphism. Int. J. Pharm. 318, 146–153.
Matteucci, M.E., Brettmann, B.K., Rogers, T.L., Elder, E.J., Williams, R.O., Johnston, K.P., 2007. Design of potent amorphous drug nanoparticles for rapid generation of highly supersaturated media. Mol. Pharmcol. 4, 782–793.
Mehramizi, A., Asgari Monfared, E., Pourfarzib, M., Bayati, K.H., Dorkoosh, F.A., Rafiee-Tehrani, M., 2007. Influence of β-cyclodextrin complexation on lovastatin release from osmotic pump tablets (OPT). Daru 15, 71–78.
Neves, N.M., Kouyumdzhiev, A., Reis, R.L., 2005. The morphology, mechanical properties and ageing behavior of porous injection molded starch-based blends for tissue engineering scaffolding. Mater. Sci. Eng. C 25, 195–200.
Norris, D.A., Puri, N., Sinko, P.J., 1998. The effect of physical barriers and properties on the oral absorption of particulates. Adv. Drug Deliv. Rev. 34, 135–154.
Nunes, C.D., Vaz, P.D., Fernandes, A.C., Ferreira, P., Romao, C.C., Calhorda, M.J., 2007. Loading and delivery of sertraline using inorganic micro and mesoporous materials. Eur. J. Pharm. Biopharm. 66, 357–365.

Oh, W.K., Yoon, H., Jang, J., 2010. Size control of magnetic carbon nanoparticles for drug delivery. Biomaterials 31, 1342–1348.
Rouquerol, J., Avnir, D., Fairbridge, C.W., Everett, D.H., Haynes, J.H., Pernicone, N., Ramsay, J.D.F., Sing, K.S.W., Unger, K.K., 1994. Recommendations for the characterization of porous solids. Pure Appl. Chem. 66, 1739.
Santander-Ortega, M.J., Stauner, T., Loretz, B., Ortega-Vinuesa, J.L., Bastos-González, D., Wenz, G., Schaefer, U.F., Lehr, C.M., 2010. Nanoparticles made from novel starch derivatives for transdermal drug delivery. J. Control Release 141, 85–92.
Shi, X.T., Wang, Y.J., Ren, L., Zhao, N.R., Gong, Y.H., Wang, D.A., 2009. Novel mesoporous silica-based antibiotic releasing scaffold for bone repair. Acta Biomater. 5, 1697–1707.
Suresh, G., Manjunath, K., Venkateswarlu, V., Satyanarayana, V., 2007. Preparation, characterization, and in vitro and in vivo evaluation of lovastatin solid lipid nanoparticles. AAPS PharmSciTech. 8, E162–E167.
Takeuchi, H., Nagira, S., Yamamoto, H., Kawwshima, Y., 2005. Solid dispersion particles of amorphous indomethacin with fine porous silica particles by using spray-drying method. Int. J. Pharm. 293, 155–164.
Tan, A., Simovic, S., Davey, A.K., Rades, T., Prestidge, C.A., 2009. Silica–lipid hybrid (SLH) microcapsules: a novel oral delivery system for poorly soluble drugs. J. Control. Release 134, 62–70.
Tran, P.H.L., Tran, H.T.T., Lee, B.J., 2008. Modulation of microenvironmental pH and crystallinity of ionizable telmisartan using alkalizers in solid dispersions for controlled release. J. Control. Release 129, 59–65.
Yiotis, A.G., Stubos, A.K., Boudouvis, A.G., Yortsos, Y.C., 2001. A 2-D pore-network model of the drying of single-component liquids in porous media. Adv. Water Resour. 24, 439–460.
Zhang, Y.Z., Zhi, Z.Z., Jiang, T.Y., Zhang, J.H., Wang, Z.Y., Wang, S.L., 2010a. Spherical mesoporous silica nanoparticles for loading and release of the poorly water-soluble drug telmisartan. J. Control. Release.
Zhang, Y.M., Hu, L.Y., Han, J.C., Jiang, Z.H., Zhou, Y.F., 2010b. Soluble starch scaffolds with uniaxial aligned channel structure for in situ synthesis of hierarchically porous silica ceramics. Micropor. Mesopor. Mater. 130, 327–332.